Journal of Geophysical Research: Atmospheres

RESEARCH ARTICLE
10.1029/2018JD028736

Special Section:
Winter INvestigation of Transport, Emissions and Reactivity (WINTER)

NO_x Lifetime and NO_y Partitioning During WINTER

Hannah S. Kenagy[1], Tamara L. Sparks[1], Carlena J. Ebben[1], Paul J. Wooldrige[1], Felipe D. Lopez-Hilfiker[2], Ben H. Lee[2], Joel A. Thornton[2], Erin E. McDuffie[3,4,5], Dorothy L. Fibiger[3,5], Steven S. Brown[3,4], Denise D. Montzka[6], Andrew J. Weinheimer[6], Jason C. Schroder[4,5], Pedro Campuzano-Jost[4,5], Douglas A. Day[4,5], Jose L. Jimenez[4,5], Jack E. Dibb[7], Teresa Campos[6], Viral Shah[2], Lyatt Jaeglé[2], and Ronald C. Cohen[1,8]

[1]Department of Chemistry, University of California, Berkeley, CA, USA, [2]Department of Atmospheric Sciences, University of Washington, Seattle, WA, USA, [3]Chemical Sciences Division, Earth System Research Laboratory, National Oceanic and Atmospheric Administration, Boulder, CO, USA, [4]Department of Chemistry and Biochemistry, University of Colorado Boulder, Boulder, CO, USA, [5]Cooperative Institute for Research in Environmental Sciences, University of Colorado Boulder, Boulder, CO, USA, [6]National Center for Atmospheric Research, Boulder, CO, USA, [7]Institute for the Study of Earth, Oceans, and Space, University of New Hampshire, Durham, NH, USA, [8]Department of Earth and Planetary Sciences, University of California, Berkeley, CA, USA

Key Points:
- NO_x is long lived during winter, with a longer daytime lifetime (29 hr) than nighttime lifetime (6.3 hr)
- Wintertime NO_x lifetime is controlled by the nighttime conversion of NO_x to HNO_3 via N_2O_5 heterogeneous chemistry
- Fifteen percent of O_3 is removed at night via the dark reactions of N_2O_5

Supporting Information:
- Supporting Information S1

Correspondence to:
R. C. Cohen,
rccohen@berkeley.edu

Citation:
Kenagy, H. S., Sparks, T. L., Ebben, C. J., Wooldrige, P. J., Lopez-Hilfiker, F. D., Lee, B. H., et al. (2018). NO_x lifetime and NO_y partitioning during WINTER. *Journal of Geophysical Research: Atmospheres*, *123*, 9813–9827. https://doi.org/10.1029/2018JD028736

Received 9 APR 2018
Accepted 18 JUL 2018
Accepted article online 1 AUG 2018
Published online 6 SEP 2018

Abstract Although urban NO_x lifetimes have been examined extensively during summertime conditions, wintertime NO_x chemistry has been comparatively less studied. We use measurements of NO_x and its oxidation products from the aircraft-based WINTER (Wintertime INvestigation of Transport, Emissions, and Reactivity) experiment over the northeastern United States during February–March 2015 to describe the NO_x lifetime during conditions when days are shorter, actinic flux is reduced, and temperatures are colder. By analyzing regional outflow from the East Coast, we show that NO_x is long lived during the winter, with a longer daytime lifetime (29 hr) than nighttime lifetime (6.3 hr). We demonstrate that wintertime NO_x emissions have an overall lifetime controlled by the *nighttime* conversion of NO_x to nitric acid (HNO_3) via N_2O_5 heterogeneous chemistry, and we discuss constraints on the rates of NO_x conversion to HNO_3. Additionally, analysis of the nighttime O_x budget suggests that approximately 15% of O_3 is lost overnight through N_2O_5 production and subsequent reaction with aerosol to form HNO_3.

Plain Language Summary The atmospheric lifetime (how long something persists in the atmosphere) and fate of nitrogen oxides in urban areas during the summer has been studied extensively, but relatively few studies have looked at the lifetime of nitrogen oxides in the atmosphere during winter. We use aircraft data from the East Coast of the United States during February–March 2015 to characterize the wintertime lifetime of nitrogen oxides when days are shorter, sunlight is reduced, and temperatures are colder. We are able to measure the wintertime lifetime of nitrogen oxides and assess the relative roles of mixing, deposition, and chemistry on their fate. We determine that nitrogen oxide loss during winter is dominated by nighttime rather than daytime chemistry and that this nighttime chemistry effectively removes ozone from the atmosphere.

1. Introduction

Nitrogen oxides ($NO_x = NO + NO_2$) influence both the gas and aerosol phases of tropospheric chemistry, with impacts on air quality, climate, and nutrient cycling in ecosystems. In the atmosphere, NO_x regulates oxidants, such as nitrate radicals (NO_3), hydroxyl radicals (OH), and ozone (O_3). Ozone is both a respiratory irritant and a greenhouse gas, and its production is a nonlinear function of NO_x concentration. Through its influence on the tropospheric oxidant budget, NO_x also controls the lifetime of greenhouse gases such as methane. Moreover, NO_x affects the formation of inorganic nitrate aerosol (e.g., Bian et al., 2017; Guo et al., 2016; Mezuman et al., 2016) and secondary organic aerosol through its impacts on tropospheric oxidation and through the formation of organic nitrates (e.g., Ayres et al., 2015; Fry et al., 2014; Rollins et al., 2012; Fisher et al., 2016; Kiendler-Scharr et al., 2016; Lee et al., 2016; L. Lee, Wooldridge, et al., 2014; Lee Ng et al., 2017).

NO_x is emitted to the atmosphere as NO both anthropogenically, through fossil fuel combustion, agriculture, and biomass burning (e.g., Dallmann & Harley, 2010; Mebust & Cohen, 2014), and naturally, from soil bacteria

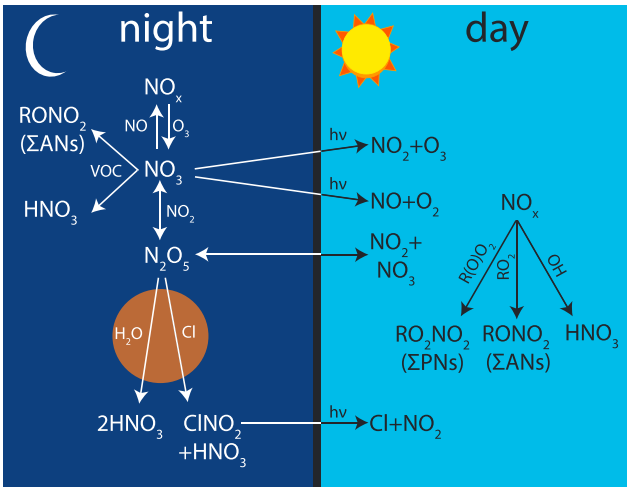

Figure 1. Schematic of NO_x oxidation reactions. The right panel contains daytime reactions, while the left panel contains nighttime reactions.

and lightning (e.g., Hudman et al., 2012; Schumann & Huntrieser, 2007). Once emitted, NO_x typically undergoes a series of oxidative transformations to higher oxides of nitrogen, some of which are then removed from the atmosphere via deposition.

In the presence of sunlight, NO_x is oxidized by HO_x radicals ($HO_x = HO_2 + RO_2 + OH$), which are produced mainly through photolytic reactions. Oxidation reactions (R1), (R2), and (R3), as shown in Figure 1, are the primary daytime NO_x sinks with the products peroxy nitrates (RO_2NO_2, noted as a class as ΣPNs), alkyl nitrates ($RONO_2$, noted as a class as ΣANs), and nitric acid (HNO_3), respectively. Depending on the conditions, these NO_x sinks may be temporary, allowing NO_x to be rereleased back to the atmosphere, or they may be permanent, with sink species eventually being deposited out of the atmosphere.

$$NO_2 + RO_2 \xrightarrow{M} RO_2NO_2(\Sigma PNs) \quad (R1)$$

$$NO + RO_2 \xrightarrow{M} RONO_2(\Sigma ANs) \quad (R2)$$

$$NO_2 + OH \xrightarrow{M} HNO_3 \quad (R3)$$

NO_3 is formed via reaction between NO_2 and O_3 (R4) and is lost via photolysis, reaction with NO, and reaction with volatile organic compounds (VOCs; e.g., Aldener et al., 2006; Liebmann, Karu, et al., 2018; Liebmann, Muller, et al., 2018). NO_3 can be an important NO_x intermediate at night when there is neither sunlight nor high concentrations of NO present to remove it. At night, NO_3 can react with another NO_2 molecule to form N_2O_5 (R5), as shown in Figure 1. Upon collision with aerosol, N_2O_5 can hydrolyze to form nitric acid (R6) or, in the presence of aerosol-phase chloride, will react to form nitryl chloride and nitric acid (R7). Alternatively, NO_3 reacts with alkenes at night (with branching ratio α) to generate alkyl nitrates (R8) and with VOCs to form nitric acid (R9). NO_3 also reacts with RO_2 and HO_2 radicals (R10) and (R11) to recycle NO_x (Stone et al., 2014).

$$NO_2 + O_3 \rightarrow NO_3 + O_2 \quad (R4)$$

$$NO_3 + NO_2 \overset{M}{\rightleftharpoons} N_2O_5 \quad (R5)$$

$$N_2O_5 + H_2O \xrightarrow{het.} 2HNO_3 \quad (R6)$$

$$N_2O_5 + HCl \xrightarrow{het.} HNO_3 + ClNO_2 \quad (R7)$$

$$NO_3 + \text{alkene} \xrightarrow{M} RONO_2(\Sigma ANs) \quad (R8)$$

$$NO_3 + VOC \xrightarrow{M} HNO_3 + \text{products} \quad (R9)$$

$$NO_3 + RO_2 \rightarrow NO_2 + RO + O_2 \quad (R10)$$

$$NO_3 + HO_2 \rightarrow NO_2 + OH + O_2 \quad (R11)$$

The rate of (R6) depends on the heterogeneous uptake coefficient for N_2O_5 ($\gamma_{N_2O_5}$). The $\gamma_{N_2O_5}$ represents the reaction probability of N_2O_5 on aerosol and depends on both aerosol composition and ambient conditions. The rate of (R7) depends on the yield for $ClNO_2$ formation, which depends on aerosol liquid water content and particulate chloride concentrations (Bertram & Thornton, 2009). At sunrise, N_2O_5 will thermally dissociate and both NO_3 and $ClNO_2$ will photolyze, thereby rereleasing NO_x.

Urban NO_x chemistry and the reaction set above have been studied extensively during summertime conditions when typical daytime NO_x lifetimes are 2–11 hr (e.g., Alvarado et al., 2010; Dillon et al., 2002; Nunnermacker et al., 2000; Romer et al., 2016; Ryerson, 2003; Ryerson et al., 1998; Valin et al., 2013). In contrast, wintertime NO_x chemistry, which we expect to differ from summertime chemistry, has been studied considerably less. Evaporative and biogenic VOC emissions are much less important in winter than in summer. The colder temperatures of wintertime slow reactions with activation barriers and accelerate three-body

Table 1
Summary of Instrumentation From the WINTER Campaign Used in This Analysis

Instrument/method	Species measured	Reference
TD-LIF[a]	NO_2, Σ ANs, Σ PNs	Day et al. (2002)
HRToF-CIMS[b]	HNO_3, N_2O_5, $ClNO_2$	Kercher et al. (2009); B. H. Lee, Lopez-Hilfiker, et al. (2014)
CRDS[c]	NO, NO_2, O_3	Fuchs et al. (2009); Wagner et al. (2011)
		Washenfelder et al. (2011); Wild et al. (2014)
	N_2O_5	Dubé et al. (2006); Fuchs et al. (2008)
		Wagner et al. (2011)
CRDS with thermal dissociation	total NO_y	Wild et al. (2014)
VUV resonance fluorescence	CO	Gerbig et al. (1999)
CL[d]	NO, O_3, total NO_y	Ridley et al. (1994)
TOGA[e]	Suite of VOCs	Apel et al. (2015)
PCASP[f]	Aerosol surface area	Strapp et al. (1992)
AMS[g]	Aerosol nitrate (PM_1)	Canagaratna et al. (2007); DeCarlo et al. (2006)
		Dunlea et al. (2009); Schroder et al. (2018)
Filter with IC[h]	Aerosol nitrate (PM_4)	Dibb et al. (1999); Dibb et al. (2000)

Note. WINTER = Wintertime INvestigation of Transport, Emissions, and Reactivity; VUV = vacuum ultraviolet; NCAR = National Center for Atmospheric Research. [a]Thermal dissociation laser-induced fluorescence (University of California, Berkeley). [b]Iodide-adduct high-resolution time-of-flight chemical ionization spectrometer (University of Washington). [c]Cavity ring down spectrometer (National Oceanic and Atmospheric Administration). [d]Chemiluminescence detector (NCAR). [e]Trace organic gas analyzer (NCAR). [f]Passive cavity aerosol spectrometer probe (NCAR). [g]Aerosol mass spectrometer (University of Colorado, Boulder). [h]Filter-sampling system used to collect PM_4 with subsequent postflight ion chromatography (University of New Hampshire).

reactions (e.g., L. Lee, Wooldridge, et al., 2014). Moreover, winter is characterized by shorter days and reduced solar radiation, causing a decrease in the role of photolysis and shifting the balance of daytime oxidation and nighttime chemistry.

Previous model and observation-based studies of wintertime chemistry have shown that a large fraction of NO_x loss occurs as a result of nighttime N_2O_5 chemistry (e.g., Alexander et al., 2009; Davis et al., 2008; Dentener & Crutzen, 1993; Evans & Jacob, 2005; Macintyre & Evans, 2010; Wagner et al., 2013; Wild et al., 2016) and that $ClNO_2$ can function as an important winter NO_x reservoir at night (Riedel et al., 2013). Crowley et al. (2011) showed that during the late autumn in southern Spain, nocturnal NO_x loss was dominated by the reaction of NO_3 with VOCs and that daytime and nighttime NO_x losses were comparable. During a wintertime field campaign in the Uintah Basin in Utah, United States (a rural region with intensive oil and gas operations), L. Lee, Wooldridge, et al. (2014) observed that alkyl nitrate formation was accelerated at low temperatures and dominated chemical NO_x loss during the snow-free winter of 2012 when there was little NO_x oxidation. Wild et al. (2016) showed that HNO_3 production via heterogeneous chemistry of N_2O_5 dominated NO_x loss during 2013 and 2014 winters when there was more NO_x oxidation in the Uintah Basin.

These prior studies show that NO_x lifetimes during winter vary and that key mechanisms depend on the interplay of emissions and meteorology. Here we explore that interplay in continental outflow to gain quantitative insights into processes and mechanisms. We use data from the 2015 aircraft-based WINTER (Wintertime INvestigation of Transport, Emissions, and Reactivity) campaign over the eastern United States to constrain the daytime and nighttime NO_x lifetime under wintertime conditions in urban environments. We determine the most important wintertime sinks of NO_x during both day and night, and we estimate wintertime rates of mixing between the boundary layer and the free troposphere and rates of HNO_3 deposition. Lastly, we investigate the impact of winter nighttime chemistry on the odd-oxygen budget.

2. Instrumentation/Measurements

The WINTER campaign took place aboard the National Science Foundation/National Center for Atmospheric Research C-130 aircraft during February and March 2015. It consisted of 13 research flights out of Norfolk, VA, which covered the eastern United States as well as the Atlantic Ocean during both day and night.

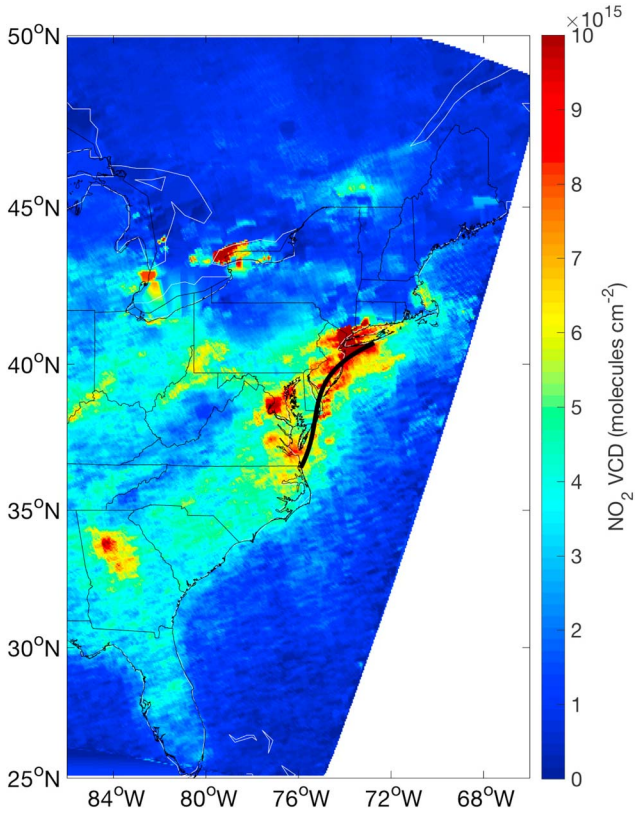

Figure 2. Ozone Monitoring Instrument satellite NO_2 vertical column density (VCD) during the Wintertime INvestigation of Transport, Emissions, and Reactivity campaign. The corridor between Washington, D.C., and New York City, represented by the black line, has high NO_2 concentrations. The outflow from this corridor moves out over the Atlantic Ocean since wind moves from west to east. For reference, 1° longitude corresponds to 85 km at 40°N.

The aircraft was outfitted with a suite of instruments measuring gas and aerosol composition. Those used in this analysis are detailed in Table 1. Additionally, the aircraft was outfitted with instrumentation measuring temperature, pressure, and wind speed. The GEOS-Chem chemical transport model (www.geos-chem.org) was run for each flight path. The WINTER campaign simulations used model version 10-01 driven by meteorological fields from NASA GMAO's GEOS-5 FP system. The model has been described in detail previously (Bey et al., 2001; Mao et al., 2010; Parrella et al., 2012; Travis et al., 2016).

3. Results and Analysis

Imagery of NO_2 vertical column density from the Ozone Monitoring Instrument satellite during the period of the WINTER campaign in Figure 2 shows that the corridor between Washington, D.C., and New York City (DC-NYC corridor) has high NO_2 concentrations relative to the surrounding regions. Here we analyze the regional outflow that moves east from the DC-NYC corridor over the Atlantic Ocean, since the average measured wind direction was 274° (i.e., from west to east), with a standard deviation of 33° (calculated using the Yamartino method; Yamartino, 1984). We then analyze the isolated outflow since there are no important sources of NO_x over the ocean aside from ship plumes, which were not sampled during the aircraft transects included in this analysis.

We parameterize the East Coast with a polynomial fit, as shown by the black line in Figure 2. We then calculate the distance of each measurement from the East Coast and use the average wind speed measured on each flight during either day or night (shown in Table 2) to calculate the time each measured air parcel originated on the East Coast. We consider coastal measurements (time 0) to be those within 25 km of the black line in Figure 2. We categorize data into day (using flights 1, 3, and 4) and night (using flights 1, 3, 4, and 6) periods, considering only points whose entire trajectory from the East Coast to location of measurement took place during daylight or darkness, respectively. During WINTER, average sunrise occurred at 06:45 and sunset at 17:30. Although flights 5 and 8 measured nighttime outflow from the DC-NYC corridor, we omit these from our analysis due to anomalously high (flight 5, mean nighttime wind speed 16.1 m/s) and anomalously low (flight 8, mean nighttime wind speed 2.7 m/s) wind speeds, compared to the mean nighttime boundary layer wind speed over the ocean during the campaign of 8.1 m/s. Flight tracks used are shown in Figure 3, and the average wind speed, temperature, and altitude sampled during each flight are shown in Table 2.

We then analyze the average concentrations of components of NO_y (NO_x, ΣPNs, ΣANs, HNO_3, N_2O_5, $ClNO_2$, and aerosol-phase NO_3^-) as a function of time elapsed since leaving the East Coast, as shown in Figure 4. In this analysis, we use chemiluminescence measurements of NO and total NO_y; thermal dissociation laser-induced fluorescence measurements of NO_2, ΣANs, and ΣPNs; high-resolution time-of-flight chemical ionization spectrometer measurements of HNO_3, N_2O_5, and $ClNO_2$; and cavity ring down spectrometer measurements

Table 2
Average (± 1σ) Wind Speeds, Temperatures, and Altitudes Sampled Below 1,000 m Over the Ocean During Flights Used in Analysis

Flight Number	Day			Night		
	Wind speed (m/s)	Temperature (K)	Altitude (m)	Wind speed (m/s)	Temperature (K)	Altitude (m)
1	6.28 ± 1.81	267.7 ± 1.3	219 ± 142	7.79 ± 1.44	267.1 ± 2.4	303 ± 216
3	9.10 ± 1.64	272.5 ± 2.2	318 ± 117	9.79 ± 2.20	271.8 ± 2.4	386 ± 182
4	4.14 ± 3.31	270.7 ± 1.7	436 ± 199	3.75 ± 1.22	276.1 ± 2.3	416 ± 126
6	—	—	—	8.96 ± 1.32	277.1 ± 2.1	350 ± 192

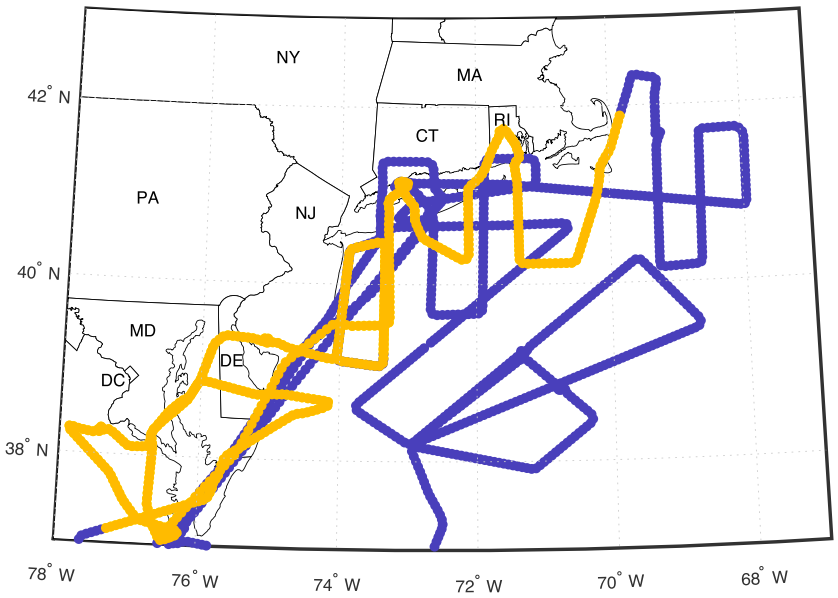

Figure 3. Map of flight tracks used in analysis of regional outflow. Blue tracks correspond to data taken at night (flights 1, 3, 4, and 6), whereas orange tracks correspond to data taken during the day (flights 1, 3, and 4). The parameterized coastline of the corridor between Washington, D.C., and New York City is shown in black. We consider coastal measurements (time 0) to be those within 25 km of this line.

of O_3. For aerosol-phase NO_3^-, we use the maximum of the aerosol mass spectrometer measurements of aerosol-phase inorganic NO_3^- and the filter-collected ion chromatography-analyzed NO_3^-. We include in Figure 4 only measurements taken in the boundary layer. We use GEOS-Chem estimates (Molod et al., 2012; Rienecker et al., 2008) of the boundary layer height (BLH) which agree with our aircraft observations of vertical profiles of relative humidity and ozone (not shown). Over the ocean during the day on flights 1, 3, and 4, the GEOS-Chem BLH was 780 m, and during the night on flights 1, 3, 4, and 6, the GEOS-Chem BLH was 610 m.

Our analysis assumes westerly winds that remain constant during a given flight but yields a regional average of the observations of the East Coast outflow. Of course, there are local variations in all of the parameters assessed hereafter, but we present an average case of the conditions during WINTER.

3.1. Daytime Chemistry

The daytime evolution of the East Coast outflow shown in Figure 4 suggests that NO_x has an *e*-folding lifetime well in excess of 10 hr during winter daytime. Within the first 7 hr of evolution, total NO_y decreases by 16% which corresponds to a cumulative loss of 1 ppb of NO_y to deposition and mixing with the free troposphere. After 7 hr of evolution, NO_x is still the dominant fraction of NO_y (80%). Fitting the decay of NO_x as a function of time elapsed since leaving the East Coast indicates that the *e*-folding lifetime for NO_x is 29 (−8, +16) hr (range of lifetime estimates described in Appendix C). This lifetime estimate accounts for NO_x loss due to chemistry, deposition, and mixing with the free troposphere. Of the NO_x sinks present in the daytime in Figure 4, HNO_3 is present in the highest concentration, which suggests that it is the primary daytime chemical NO_x sink.

We then calculate the production rates of each daytime NO_x sink compound over the ocean, as described in Appendix A. We find that the average (± 95% confidence interval) $P(\Sigma ANs)$ is 0.39 (± 0.07) ppt/hr, the average $P(\Sigma PNs)$ is 5.1 (± 0.4) ppt/hr, and the average $P(HNO_3)$ is 50 (± 4) ppt/hr, using GEOS-Chem estimates of OH concentrations (average 0.01 ppt in boundary layer). These production rates confirm that ΣANs and ΣPNs are relatively unimportant daytime NO_x sinks, whereas HNO_3 production is the dominant, albeit small, daytime NO_x sink reaction pathway.

3.2. Nighttime Chemistry

The nighttime outflow evolution shown in Figure 4 demonstrates that NO_x is shorter lived at night than during the day. Fitting the decay of NO_x as a function of time elapsed since leaving the East Coast yields an *e*-folding lifetime of 6.3 (−0.5, +0.6) hr, which takes into account both chemical and physical loss processes. Initially, NO_x is the dominant component (75%) of NO_y. Fifty percent (4.5 ppb) of NO_y is lost to deposition and mixing

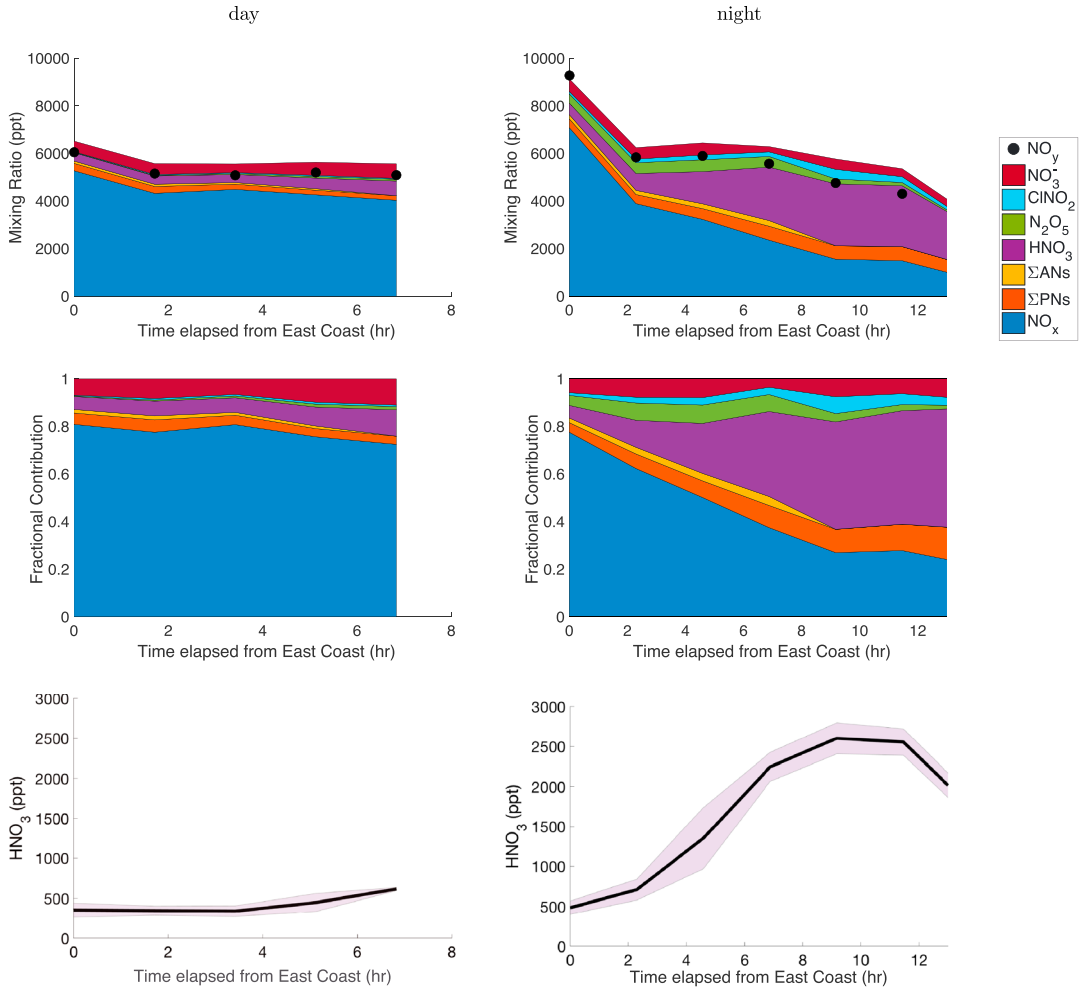

Figure 4. Mixing ratios (top row) of species contributing to NO_y, fractional contribution (middle row) of species contributing to NO_y, and growth of HNO_3 (bottom row) during daytime hours (left column) and nighttime hours (right column) shown as a function time elapsed from the East Coast. Time elapsed from the East Coast is calculated by dividing the distance of each measurement from the East Coast by the average wind speed measured on each flight. Data are then binned and averaged as a function of time elapsed (day bins = 1.7 hr; night bins = 2.3 hr). In the bottom row, shading represents a 95% confidence interval. Flights 1, 3, and 4 are used in daytime calculations, and flights 1, 3, 4, and 6 are used in nighttime calculations. Only boundary layer data are included (below 780 m during the day and below 610 m at night).

with the free troposphere during the first 9 hr of evolution, and after 9 hr of evolution, HNO_3 is the dominant fraction (55%) of NO_y.

At night, there is evidence of NO_x conversion to NO_3, N_2O_5, ΣANs, HNO_3, and $ClNO_2$. Of these nighttime NO_x sinks, on average HNO_3 is present in the highest concentration. There was significant variation observed during different flights in the ratio of $ClNO_2$ to HNO_3 (nighttime boundary layer outflow average = 0.26, standard deviation = 0.44), which is not captured in the averages shown in Figure 4. We calculate the average production rate of HNO_3 (equation (B1)) from N_2O_5 reactions on aerosol surfaces over the ocean at night, as described in Appendix B, assuming a constant $ClNO_2$ yield. We find the average $P(HNO_3)$ at night to be 350 (± 30) ppt/hr, 7 times the daytime $P(HNO_3)$ of 50 ppt/hr (Table 3).

4. Two-Box Model to Constrain Mixing and Deposition Rates

To understand if the chemistry described above is sufficient to describe the observations, we construct a two-box model with detailed chemistry and observationally constrained initial conditions and solve iteratively to estimate mixing rates between the boundary layer and the free troposphere (k_{mix}), the heterogeneous

Table 3
Summary of Calculated Parameters Related to NO_x Lifetime During the Daytime and Nighttime

	Day	Night
NO_x lifetime (hr)	29	6.3
$P(HNO_3)$ (ppt/hr)	50	350

Note. Production rates of sinks with only minor contributions to the NO_x lifetime are not shown.

uptake coefficient for N_2O_5 ($\gamma_{N_2O_5}$), and the rate of HNO_3 deposition ($k_{dep}(HNO_3)$). The bottom of the two boxes represents the boundary layer, with chemistry occurring at 273 K and 1,000 hPa, and the top box represents the free troposphere, with chemistry occurring at 253 K and 600 hPa. These temperatures and pressures are representative of average conditions during WINTER and are shown schematically in Figure 5. During WINTER, the continental air advecting over the ocean is colder than the water at the ocean's surface. This generates a convective mixing process that leads to a relatively deep marine boundary layer, making a two-box model appropriate for this analysis.

Reaction rates used in the model are detailed in the supporting information and were obtained from Burkholder et al. (2015), Master Chemical Mechanism v. 3.3.1 (Bloss et al., 2005; Jenkin et al., 2015; Jenkin et al., 2003; Jenkin et al., 1997; Saunders et al., 2003), Wilson et al. (2006), Tyndall et al. (2001), and Atkinson et al. (2006). For model runs representing daytime conditions, the reaction of NO_2 with OH (R3) is included and the model is run for 11 hr (average length of day during WINTER). HNO_3 photolysis is neglected since the average HNO_3 photolysis frequency measured during WINTER flights 1, 3, and 4 corresponds to a photolysis lifetime exceeding 10^3 hr. For model runs representing nighttime conditions, reactions (R4)–(R8) (with included alkenes: butene, isoprene, α-pinene, and β-pinene), and (R9) (with included VOCs: methane, ethane, propane, formaldehyde, acetaldehyde, propanal, butanal, methacrolein, ethyl benzene, o-xylene, m-xylene, p-xylene, 1,2,4-trimethyl benzene, 1,2,3-trimethyl benzene, and dimethyl sulfide) are included and the model is run for 13 hr (average length of night during WINTER).

Aerosol nitrate is not included in the box model analysis because there is no net partitioning of gas-phase nitric acid into aerosol nitrate observed during the evolution of the average outflow. Aerosol nitrate remains as 10% of total NO_y throughout the outflow, as seen in Figure 4. Because aerosol deposition is slow (~ 1 week) on the time scales of our model (~ hours), the constant proportion of NO_y as aerosol nitrate indicates that any change in aerosol nitrate concentration is purely a product of dilution/mixing (i.e., not from net movement of gas phase nitric acid into aerosol). Nitric acid remains in the gas phase because of low aerosol pH (Guo et al., 2016). Consequently, aerosol nitrate does not affect the net NO_x loss on the time scales of our model.

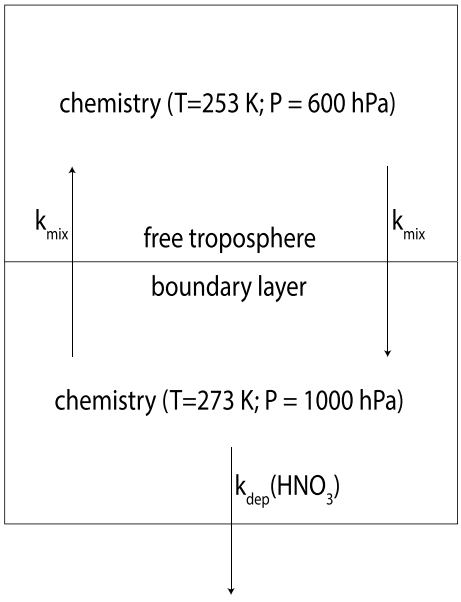

Figure 5. Schematic of the overall processes represented in the two-box model. k_{mix} represents the mixing rate of air between the boundary layer and the free troposphere. Chemistry occurs in both the boundary layer and the free troposphere, at temperatures and pressures representative of average conditions. HNO_3 has a deposition rate $k_{dep}(HNO_3)$.

Nighttime heterogeneous hydrolysis of N_2O_5 (R6) is included with rate $\frac{1}{4} \times \bar{c}N_2O_5 \times SA \times \gamma_{N_2O_5} \times [N_2O_5]$ (see Appendix B). Aerosol surface area (SA) was held constant at the median wet aerosol SA measured over the ocean during WINTER (200 $\mu m^2/cm^3$ in boundary layer, 27 $\mu m^2/cm^3$ in free troposphere), though there was significant variation in the observed aerosol SA. SA of sea salt aerosol (approximated as SA of supermicron aerosols) were estimated to be 3% of total aerosol SA in the DC-NYC outflow, so the heterogeneous reaction of N_2O_5 with chloride-containing aerosol is represented by $0.03 \times \frac{1}{4} \times \bar{c}N_2O_5 \times SA \times \gamma_{N_2O_5} \times [N_2O_5]$, ignoring chlorine displacement from sea spray and assuming that $\gamma_{N_2O_5}$ does not vary significantly with sea salt content.

Initial conditions for all species in the model are set using the average measurements at the East Coast between Washington, D.C., and New York City. OH concentrations during the day are fixed to the average OH concentration estimated by GEOS-Chem (0.01 ppt in the boundary layer; 0.04 ppt in the free troposphere). Schroder et al. (2018) determined the GEOS-Chem estimates of OH to be reasonable in the NYC plume. Exchange of all species between boxes is allowed to represent mixing between the boundary layer and the free troposphere, and HNO_3 is removed from the bottom box via deposition.

We estimate the mixing rate (k_{mix}) by iteratively adjusting k_{mix} and solving the model until the model-to-observation percent root-mean-square deviation is minimized for CO. CO chemistry is negligible on the time scales included in our model, so it is only affected by mixing between the boundary layer and the free troposphere and by horizontal dispersion. Setting initial CO concentrations to the average measurements at the East Coast

(161 ppb in the boundary layer and 98 ppb in the free troposphere) and solving iteratively yields a daytime estimate of the mixing lifetime of 24 hr and a nighttime estimate of the mixing lifetime of 15 hr. We attribute the difference in mixing lifetimes between night and day to a difference in observed wind speed. The median horizontal wind speed in the DC-NYC outflow during the day was 6.5 m/s, whereas the median horizontal wind speed at night was 8.3 m/s. The average vertical gust component of the wind vector in the regional outflow was also larger at night (−0.14 m/s) than during the day (−0.082 m/s). A larger wind speed at night, which has been observed previously off the coast of the northeast United States (Archer et al., 2016), would generate more turbulence and decrease the mixing lifetime. Additionally, during winter, the ocean surface temperature is typically warmer than the cold air outflow. At night this temperature gradient is larger, generating vertical instability and convective mixing (Archer et al., 2016).

During nighttime model runs, the heterogeneous uptake coefficient of N_2O_5 ($\gamma_{N_2O_5}$) was then estimated by iteratively adjusting $\gamma_{N_2O_5}$ while holding k_{mix} constant and solving the model until model-to-observation percent root-mean-square deviation is minimized for N_2O_5. This step was not done for the daytime version of the model since N_2O_5 chemistry is not relevant during the day. We estimate $\gamma_{N_2O_5} = 0.013$. This compares reasonably with the wintertime N_2O_5 uptake coefficients derived by McDuffie et al. (2018) for the entire WINTER campaign which ranged over 4 orders of magnitude with a median of 0.0143 and a most frequent value of 0.018. Over the ocean, McDuffie et al. (2018) derived a median N_2O_5 uptake coefficient of 0.017. McDuffie et al. (2018) also explore correlations between $\gamma_{N_2O_5}$ and both aerosol composition and meteorological conditions and compare observed values of $\gamma_{N_2O_5}$ during WINTER to available literature parameterizations. Fibiger et al. (2018) derived a very low uptake coefficient of 7×10^{-4} in a coal-fired power plant plume in Georgia during WINTER, but the low values observed in Georgia were not representative of the average values derived for flights over the ocean.

Finally, we estimate the deposition rate of HNO_3 ($k_{dep}(HNO_3)$) by varying $k_{dep}(HNO_3)$ iteratively while holding k_{mix} and (at night) $\gamma_{N_2O_5}$ constant until the maximum HNO_3 in the model matches the maximum observed HNO_3. Our model analysis constrains the deposition lifetime of HNO_3 to 29 hr during the day and 20 hr at night. Like for the trend in k_{mix}, a larger wind speed at night generates more turbulence and increases the nighttime deposition rate of HNO_3.

Our estimation of the daytime deposition rate of HNO_3 is sensitive to model uncertainty in OH concentrations. Our estimation of the nighttime deposition rate of HNO_3 is linked to the yield of $ClNO_2$ from N_2O_5 heterogeneous reactions. In our model, we use a constant sea salt aerosol fraction as an estimate of $ClNO_2$ yield and assume a constant $\gamma_{N_2O_5}$ that does not vary with sea salt content. These constant parameters do not account for the observed variability in the $ClNO_2/HNO_3$ ratio. Additionally, if the sea salt aerosol fraction underestimates (overestimates) the $ClNO_2$ yield or if a single $\gamma_{N_2O_5}$ value underestimates (overestimates) $\gamma_{N_2O_5}$ on chloride-containing aerosols, $k_{dep}(HNO_3)$ will be overestimated (underestimated). Moreover, we do not include deposition of N_2O_5 nor $ClNO_2$ to the ocean in our model, which could lead to an overestimation of $\gamma_{N_2O_5}$ and a slight overestimation of HNO_3 production, resulting in an overestimation of $k_{dep}(HNO_3)$.

We estimate the deposition velocity (v_{dep}) of HNO_3 as

$$v_{dep} = BLH \times k_{dep}(HNO_3) \quad (1)$$

using GEOS-Chem estimates of the BLH. Over the ocean during the day on flights 1, 3, and 4, the GEOS-Chem BLH was 780 m, yielding a deposition velocity of 0.75 cm/s. Over the ocean during the night on flights 1, 3, 4, and 6, the GEOS-Chem BLH was 610 m, yielding a deposition velocity of 0.85 cm/s. Similarly, Brown et al. (2004) calculated a nitric acid deposition velocity of 1.2 cm/s off the East Coast of the United States during summer. However, despite similar deposition velocities during both seasons, more nitric acid is deposited in coastal marine environments during winter than during summer. In summer, warm continental air advects over cold water, which isolates the shallow marine boundary layer and allows for long-distance transport above the boundary layer where it is not subject to deposition near the coast (Neuman et al., 2006). In contrast, during winter, cold air advects over warmer water which generates mixing and leads to a deeper marine boundary layer (Seidel et al., 2012) that allows for significant coastal nitric acid deposition.

A summary of the parameters included in the final two-box model is shown in Table 4, and the outputs of the two-box model with these parameters along with average observations are shown in Figure 6. The output indicates that daytime chemistry can be described with reasonable accuracy by considering HNO_3 as the only chemical sink of NO_x. The nighttime model captures the conversion of NO_x to NO_3, N_2O_5, ΣANs, HNO_3,

Table 4
Table of Parameters Included in Box Model

	Day		Night	
	Boundary layer	Free troposphere	Boundary layer	Free troposphere
[OH] (ppt)	0.01	0.04	—	—
SA ($\mu m^2/cm^3$)	—	—	200	27
T (K)	273	253	273	253
P (hPa)	1,000	600	1,000	600
k_{dep} (HNO_3) (hr^{-1})	1/29	—	1/20	—
k_{mix} (hr^{-1})	1/24	1/24	1/15	1/15
$\gamma(N_2O_5)$	—	—	0.013	0.013

and $ClNO_2$, with HNO_3 as the major NO_x sink. During both day and night, NO_y loss in the boundary layer is dominated by mixing into the free troposphere rather than by deposition.

5. Integrated NO_x Loss and Impacts on Odd-Oxygen Budget

We integrate the production rates of each NO_x sink in our two-box model over the course of 24 hr, with 11 hr of day and 13 hr of night, to calculate the integrated NO_x loss via each reaction. HNO_3 has the largest integrated production and is thus the largest sink of NO_x. However, the nighttime multiphase N_2O_5 chemistry that converts NO_x to HNO_3 has a more significant impact than the photochemical daytime reaction of NO_2 with OH that leads to HNO_3 production. During the day, 10% of initial NO_x (500 ppt) is lost to HNO_3, whereas 64% (4,500 ppt) of initial nighttime NO_x is converted to HNO_3 overnight via N_2O_5 chemistry. At night, an additional 0.7% of initial NO_x (50 ppt) is lost to HNO_3 from reaction of NO_3 with VOCs and dimethyl sulfide, 0.9% of initial NO_x (60 ppt) is lost to alkyl nitrates produced via NO_3 reaction with alkenes, and 1.2 % of initial NO_x (90 ppt) is converted to $ClNO_2$ via heterogeneous chemistry of N_2O_5 on sea salt aerosol (though $ClNO_2$ concentrations did vary significantly between flights, indicating variation in $ClNO_2$ yield not accounted for in our analysis). In the summer marine boundary layer off the East Coast of the United States, only one third of HNO_3 production occurs during the night (Brown et al., 2004), whereas during the East Coast outflow measured during WINTER, 90% of HNO_3 production occurs at night. The boundary layer is ~ 25% shallower at night than during the day (610 m at night vs. 780 m during the day). This is not enough of a difference to perturb the balance of nighttime chemistry dominating NO_x loss even after accounting for the volume over which the processes occur. Thus, in contrast to summertime when NO_x chemistry is controlled by daytime photochemistry with OH serving as the primary oxidant, wintertime NO_x loss is dominated by nighttime multiphase oxidation with O_3 as the primary oxidant.

Most wintertime oxidation of NO_x leads to the formation of HNO_3, which is then eventually deposited. Formation of peroxy nitrates is found to be negligible and have little effect in the near coastal region. However,

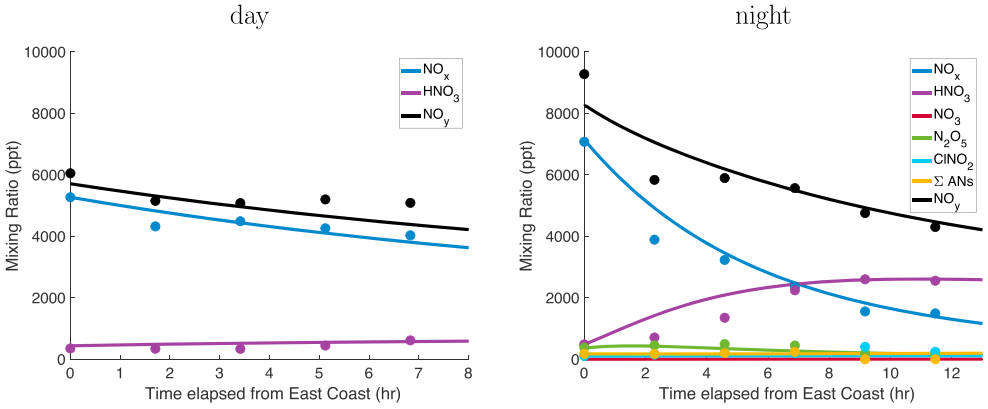

Figure 6. Concentrations in the boundary layer calculated in the two-box model (lines) and average concentrations measured in the Washington, D.C.-New York City outflow (points) during the day (left) and at night (right).

some of the nighttime NO_x sinks are temporary and rerelease NO_x when they are photolyzed or thermally dissociated at sunrise. The amount of NO_x rereleased in the morning corresponds to the amount of NO_x stored in NO_3, N_2O_5, and $ClNO_2$ reservoirs. In our model, after one night of chemical evolution following emission, these NO_x reservoirs contain 400 ppt of NO_x (6% of NO_x concentration at East Coast), which is rereleased in the morning.

O_3 is lost overnight through conversion of NO_x to HNO_3 via N_2O_5 dark reactions (R4), (R5), and (R6). When HNO_3 is produced via heterogeneous hydrolysis of N_2O_5 (R6), the dominant NO_x loss mechanism at night, each molecule of HNO_3 generated corresponds to a loss of 1.5 molecules of O_3 (Brown et al., 2006). In our two-box model, 4,400 ppt of HNO_3 is produced overnight through N_2O_5 hydrolysis, implying a loss of 6,600 ppt of O_3 overnight. The average nighttime O_3 concentration in the DC-NYC outflow is 38 ppb, so approximately 15% of O_3 is lost overnight through N_2O_5 dark reactions. O_3 concentrations in the boundary layer remain relatively constant throughout the region at night. This is because chemical loss of O_3 is roughly balanced by mixing down of higher O_3 concentrations from the free troposphere (49 ppb at the East Coast). This balance was confirmed by our model runs.

Photochemical O_3 production is reduced in the winter when compared to summer because of low sun angles and reduced daylight hours with precursor concentrations that are only slightly elevated. In addition to reduced O_3 production, we infer significant boundary layer loss of O_3 in the East Coast outflow resulting from nighttime NO_x chemistry during winter. The presence of VOCs influences the balance between daytime O_3 production and nighttime O_3 loss, as VOCs are required for photochemical O_3 production and can also react with NO_3 to destroy O_3 at night. The extent of nocturnal O_3 destruction is also dependent on the concentrations and composition of aerosol particles, since these affect the rate of heterogeneous reactions of N_2O_5.

6. Conclusions

Analysis of the DC-NYC marine outflow indicates that NO_x has a longer daytime lifetime (29 hr) than nighttime lifetime (6.3 hr) during winter. We constrain the rates of the chemical and physical loss processes that contribute to the overall NO_x lifetime during winter in urban areas. Chemically, we conclude that HNO_3 is the primary NO_x sink during both day and night, whereas peroxy nitrates and alkyl nitrates are relatively small NO_x sinks since VOC reactivity is so low. Thus, the wintertime NO_x lifetime is controlled primarily by HNO_3 production, and nighttime chemistry removes more NO_x than does daytime chemistry. The shorter days and reduced sunlight characteristic of winter slow daytime chemistry by reducing OH concentrations and, consequently, VOC reactivity. At night, a shallower planetary boundary layer increases NO_x concentrations, thereby increasing the importance of N_2O_5 chemistry which scales with the square of NO_x concentration (R4) and (R5). Additionally, colder temperatures shift N_2O_5 equilibrium to the right, further increasing the importance of nighttime chemistry. Physically, we estimate a winter daytime mixing rate of 24 hr, a nighttime mixing rate of 15 hr, a daytime HNO_3 deposition lifetime of 29 hr, and a nighttime HNO_3 deposition lifetime of 20 hr. Lastly, we observe that approximately 15% of O_3 is removed at night via the dark reactions of N_2O_5, demonstrating that urban NO_x emissions impact O_3 concentrations differently in summer versus in winter.

Appendix A: Daytime Production Rate Calculations

We calculate the daytime production of alkyl nitrates via reaction (R2) as

$$P(\Sigma\text{ANs}) = \sum_i \alpha_i f_{NO_i} k_{OH+RH_i}[OH][RH_i] \tag{A1}$$

where

$$f_{NO_i} = \frac{k_{RO_{2i}+NO}[NO]}{k_{RO_{2i}+NO}[NO] + k_{RO_{2i}+HO_2}[HO_2] + k_{RO_{2i}+RO_2}[RO_2]} \approx 1 \text{during WINTER} \tag{A2}$$

We approximate $f_{NO} \approx 1$ since $[NO] \gg [HO_2]$, $[RO_2]$ during WINTER. We use the following VOCs: methane, ethane, propane, n-butane, n-pentane, i-butane, i-pentane, 2-methyl pentane, 3-methyl pentane, n-hexane, n-heptane, isoprene, methacrolein, methyl vinyl ketone, α-pinene, β-pinene, butanal, 1-butene, benzene, toluene, o-xylene, m-xylene, p-xylene, ethyl benzene, 1,2,4-trimethyl benzene, and 1,2,3-trimethyl benzene

(Perring et al., 2013). All α values were taken from Perring et al. (2013). We calculate the daytime production of peroxy nitrates as (LaFranchi et al., 2009)

$$P(\Sigma\text{PNs}) = \beta \times \alpha_{CH_3CHO} \times k_{CH_3CHO} \times [OH][CH_3CHO] \quad \text{(A3)}$$

where

$$\beta = \frac{k_{RC(O)O_2+NO_2}[NO_2]}{k_{RC(O)O_2+NO_2}[NO_2] + k_{RC(O)O_2+NO}[NO] + k_{RC(O)O_2+HO_2}[HO_2] + k_{RC(O)O_2+RO_2}[RO_2]} \quad \text{(A4)}$$

We estimate $[RO_2]$ as (Browne et al., 2013)

$$[RO_2] = \frac{-k_{HO_2+RO_2}[HO_2] - k_{NO+RO_2}[NO] + \sqrt{(k_{HO_2+RO_2}[HO_2] + k_{NO+RO_2}[NO])^2 + 8 \times k_{RO_2+RO_2} \times P(RO_2)}}{4 \times k_{RO_2+RO_2}} \quad \text{(A5)}$$

We calculate daytime production of nitric acid as

$$P(HNO_3) = k_{OH+NO_2}[OH][NO_2] \quad \text{(A6)}$$

Appendix B: Nighttime Production Rate Calculations

We calculate the average production rate of HNO_3 (equation (B1)) from N_2O_5 reactions on aerosol surfaces at night as 2 times the rate of (R6) plus the rate of (R7) since (R6) produces two molecules of nitric acid for each molecule of N_2O_5 consumed and (R7) produces one molecule of nitric acid for each molecule of N_2O_5 consumed:

$$P(HNO_3) = \frac{1}{4} \times \bar{c}_{N_2O_5} \times \gamma_{N_2O_5} \times [N_2O_5] \times (2 \times SA + SA_{\text{sea salt}}) \quad \text{(B1)}$$

Here $\bar{c}_{N_2O_5}$ represents the mean molecular speed of N_2O_5 and $\gamma_{N_2O_5}$ represents the heterogeneous uptake coefficient for N_2O_5. The rate of (R6) is proportional to the wet SA of aerosol particles, and the rate of (R7) is proportional to the SA of chloride-containing aerosol particles ($SA_{\text{sea salt}}$). This rate is valid for small values of $\gamma_{N_2O_5}$ and small particles (i.e., not diffusion-limited regimes; Sutugin & Fuchs, 1970).

We estimate $\gamma_{N_2O_5}$ using our two-box model described in Section 4. For simplicity, we use the same $\gamma_{N_2O_5}$ for all aerosols regardless of sea salt content, though this coefficient can vary.

Wet aerosol SA is calculated using the dry aerosol SA measured by the passive cavity aerosol spectrometer probe corrected for hygroscopic growth. We estimate the wet aerosol SA by applying growth factors as a function of the measured relative humidity. The growth factors are calculated with the E-AIM model (http://www.aim.env.uea.ac.uk/aim/aim.php) assuming that the submicron aerosol is composed of NH_4NO_3. We use the median wet aerosol SA over the ocean for SA, though there was variation in the observed aerosol SA.

We use the average fraction of total aerosol SA that is attributable to sea salt aerosols as a simple proxy for $ClNO_2$ yield, though chlorine can be displaced from sea spray and repartitioned into smaller aerosol particles, and there are additional factors that contribute to $ClNO_2$ yield (e.g., Bertram & Thornton, 2009; Wagner et al., 2012; Riedel et al., 2013). To estimate the SA of sea salt aerosols ($SA_{\text{sea salt}}$), we assume that sea salt mass is concentrated in the supermicron particle size range. Particles with diameter 1–10 μm (supermicron) contribute an average of 3% (± 3%, 1 standard deviation) to the total aerosol SA at night over the ocean during WINTER, so we define $SA_{\text{sea salt}} = 0.03 \times SA$. This approach does not account for any variation in the $ClNO_2$ yield and may underestimate $ClNO_2$ yield because it ignores any contribution of submicron chloride-containing aerosols to $ClNO_2$ formation. Submicron aerosols dominate urban aerosol SA and, consequently, dominate N_2O_5 uptake onto aerosols.

Appendix C: Uncertainty Calculations

We estimate the range of NO_x *e*-folding lifetimes (τ_{total}, accounting for both physical and chemical loss processes) using the bivariate York fitting method (York et al., 2004) which accounts for variability in both the *x* and *y* variables. We assume variability in *x* (time elapsed from East Coast) is dominated by the variation in wind

speed during a given flight. The average fractional 1σ variation in wind speed within each day or night subset of each flight used in this analysis was 30%, so we assign a fractional uncertainty of 30% in x. We estimate variability in y ($[NO_x]$) as the 1σ variation in the observed NO_x concentration in each time bin.

Since HNO_3 is the dominant sink of NO_x during both day and night, we assume that variability in the chemical lifetime of NO_x ($\tau_{chem.}$) is dominated by variation in the rate of conversion of NO_x to HNO_3. We assume that the uncertainty in the daytime chemical lifetime of NO_x lost to HNO_3 is dominated by uncertainty in modeled OH concentrations which we estimate as 1σ variation in modeled [OH]. We estimate the variability in the nighttime chemical lifetime of NO_x from uncertainties in [NO], $[NO_2]$, $[N_2O_5]$, aerosol SA, and $\gamma_{N_2O_5}$. We incorporate chemiluminescence instrument uncertainty for [NO] = 10% (Ridley et al., 1994), thermal dissociation laser-induced fluorescence instrument uncertainty for $[NO_2]$ = 10% (Day et al., 2002), high-resolution time-of-flight chemical ionization spectrometer instrument uncertainty for $[N_2O_5]$ = 30% (B. H. Lee, Lopez-Hilfiker, et al., 2014; Kercher et al., 2009), and passive cavity aerosol spectrometer probe uncertainty for aerosol SA = 41% (Strapp et al., 1992).

We have defined the *e*-folding lifetime of NO_x and the chemical lifetime of NO_x as first order with respect to the concentration of NO_x, but we have defined the mixing lifetime of NO_x as first order with respect to the concentration gradient of NO_x between the boundary layer (BL) and the free troposphere (FT). If we make the assumption that $[NO_x]_{FT} \ll [NO_x]_{BL}$ such that $[NO_x]_{BL}$ - $[NO_x]_{FT} \approx [NO_x]_{BL}$, then

$$\frac{1}{\tau_{total}} = \frac{1}{\tau_{chem.}} + \frac{1}{\tau_{mix}} \tag{C1}$$

Accounting for the estimated variability in τ_{total} and $\tau_{chem.}$, we estimate the variability in τ_{mix} to be 8.2 hr during the day and 10.7 hr at night.

Acknowledgments
This work was funded by the National Science Foundation NSF (AGS 1360761). Additional support was provided by a NSF Graduate Research Fellowship to H. S. K. (DGE 1106400). F. D. L. H., B. H. L., J. A. T., V. S., and L. J. were supported by NSF AGS 1360745. J. C. S., P. C. J., D. A. D., and J. L. J. were supported by NSF AGS 1360834. We thank the entire WINTER science team, and we thank Eric Apel of NCAR for the TOGA data. All data from the WINTER campaign are available at http://data.eol.ucar.edu/master_list/?project=WINTER.

References

Aldener, M., Brown, S. S., Stark, H., Williams, E. J., Lerner, B. M., Kuster, W. C., et al. (2006). Reactivity and loss mechanisms of NO_3 and N_2O_5 in a polluted marine environment: Results from in situ measurements during New England Air Quality Study 2002. *Journal of Geophysical Research*, *111*, D23S73. https://doi.org/10.1029/2006JD007252

Alexander, B., Hastings, M. G., Allman, D. J., Dachs, J., Thornton, J. A., & Kunasek, S. A. (2009). Quantifying atmospheric nitrate formation pathways based on a global model of the oxygen isotopic composition ($\Delta^{17}O$) of atmospheric nitrate. *Atmospheric Chemistry and Physics*, *9*(2), 5043–5056. https://doi.org/10.5194/acp-9-5043-2009

Alvarado, M. J., Logan, J. A., Mao, J., Apel, E., Riemer, D., Blake, D., et al. (2010). Nitrogen oxides and PAN in plumes from boreal fires during ARCTAS-B and their impact on ozone: An integrated analysis of aircraft and satellite observations. *Atmospheric Chemistry and Physics*, *10*, 9739–9760. https://doi.org/10.5194/acp-10-9739-2010

Apel, E. C., Hornbrook, R. S., Hills, A., Blake, N., Barth, M., Weinheimer, A. J., et al. (2015). Upper tropospheric ozone production from lightning NO_x-impacted convection: Smoke ingestion case study from the DC3 campaign. *Journal of Geophysical Research: Atmospheres*, *120*, 2505–2523. https://doi.org/10.1002/2014JD022121

Archer, C. L., Colle, B. A., Veron, D. L., Veron, F., & Sienkiewicz, M. J. (2016). On the predominance of unstable atmospheric conditions in the marine boundary layer offshore of the U.S. northeastern coast. *Journal of Geophysical Research: Atmospheres*, *121*, 8869–8885. https://doi.org/10.1002/2016JD024896

Atkinson, R., Baulch, D. L., Cox, R. A., Crowley, J. N., Hampson, R. F., Hynes, R. G., et al. (2006). Evaluated kinetic and photochemical data for atmospheric chemistry: Volume II—Gas phase reactions of organic species. *Atmospheric Chemistry and Physics*, *6*(11), 3625–4055. https://doi.org/10.5194/acp-6-3625-2006

Ayres, B. R., Allen, H. M., Draper, D. C., Brown, S. S., Wild, R. J., Jimenez, J. L., et al. (2015). Organic nitrate aerosol formation via NO_3 + biogenic volatile organic compounds in the southeastern United States. *Atmospheric Chemistry and Physics*, *15*(23), 13,377–13,392. https://doi.org/10.5194/acp-15-13377-2015

Bertram, T. H., & Thornton, J. A. (2009). Toward a general parameterization of, N_2O_5 reactivity on aqueous particles: The competing effects of particle liquid water, nitrate and chloride. *Atmospheric Chemistry and Physics*, *9*, 8351–8363. https://doi.org/10.5194/acp-9-8351-2009

Bey, I., Jacob, D. J., Yantosca, R. M., Logan, J. A., Field, B. D., Fiore, A. M., et al. (2001). Global modeling of tropospheric chemistry with assimilated meteorology: Model description and evaluation. *Journal of Geophysical Research*, *106*(D19), 23,073–23,095. https://doi.org/10.1029/2001JD000807

Bian, H., Chin, M., Hauglustaine, D. A., Schulz, M., Myhre, G., Bauer, S. E., et al. (2017). Investigation of global particulate nitrate from the AeroCom phase III experiment. *Atmospheric Chemistry and Physics*, *17*, 12911–12940. https://doi.org/10.5194/acp-17-12911-2017

Bloss, C., Wagner, V., Jenkin, M. E., Volkamer, R., Bloss, W. J., Lee, J. D., et al. (2005). Development of a detailed chemical mechanism (MCMv3.1) for the atmospheric oxidation of aromatic hydrocarbons. *Atmospheric Chemistry and Physics*, *5*, 641–664. https://doi.org/10.5194/acp-5-641-2005

Brown, S. S., Dibb, J. E., Stark, H., Aldener, M., Vozella, M., Whitlow, S., et al. (2004). Nighttime removal of NO_x in the summer marine boundary layer. *Geophysical Research Letters*, *31*, L07108. https://doi.org/10.1029/2004GL019412

Brown, S. S., Neuman, J. A., Ryerson, T. B., Trainer, M., Dubé, W. P., Holloway, J. S., et al. (2006). Nocturnal odd-oxygen budget and its implications for ozone loss in the lower troposphere. *Geophysical Research Letters*, *33*, L08801. https://doi.org/10.1029/2006GL025900

Browne, E. C., Min, K. E., Wooldridge, P. J., Apel, E. C., Blake, D. R., Brune, W. H., et al. (2013). Observations of total $RONO_2$ over the boreal forest: NO_x sinks and HNO_3 sources. *Atmospheric Chemistry and Physics*, *13*(9), 4543–4562. https://doi.org/10.5194/acp-13-4543-2013

Burkholder, J. B., Sander, S. P., Abbatt, J. P. D., Barker, J. R., Huie, R. E., Kolb, C. E., et al. (2015). Chemical kinetics and photochemical data for use in atmospheric studies (*Evaluation No. 18, Tech. rep.*) Pasadena: Jet Propulsion Laboratory.

Canagaratna, M., Jayne, J., Jimenez, J., Allan, J., Alfarra, M., Zhang, Q., et al. (2007). Chemical and microphysical characterization of ambient aerosols with the aerodyne aerosol mass spectrometer. *Mass Spectrometry Reviews*, *26*, 185–222. https://doi.org/10.1002/mas.20115

Crowley, J. N., Thieser, J., Tang, M. J., Schuster, G., Bozem, H., Beygi, Z. H., et al. (2011). Variable lifetimes and loss mechanisms for NO_3 and N_2O_5 during the DOMINO campaign: Contrasts between marine, urban and continental air. *Atmospheric Chemistry and Physics*, *11*(21), 10,853–10,870. https://doi.org/10.5194/acp-11-10853-2011

Dallmann, T. R., & Harley, R. A. (2010). Evaluation of mobile source emission trends in the United States. *Journal of Geophysical Research*, *115*, D14305. https://doi.org/10.1029/2010JD013862

Davis, J. M., Bhave, P. V., & Foley, K. M. (2008). Parameterization of N_2O_5 reaction probabilities on the surface of particles containing ammonium, sulfate, and nitrate. *Atmospheric Chemistry and Physics*, *8*, 5295–5311. https://doi.org/10.5194/acp-8-5295-2008

Day, D. A., Wooldridge, P. J., Dillon, M. B., Thornton, J. A., & Cohen, R. C. (2002). A thermal dissociation laser-induced fluorescence instrument for in situ detection of NO_2, peroxy nitrates, alkyl nitrates, and HNO_3. *Journal of Geophysical Research*, *107*(D6), 4046. https://doi.org/10.1029/2001JD000779

DeCarlo, P. F., Kimmel, J. R., Trimborn, A., Northway, M. J., Jayne, J. T., Aiken, A. C., et al. (2006). Field-deployable, high-resolution, time-of-flight aerosol mass spectrometer. *Analytical Chemistry*, *78*(24), 8281–8289. https://doi.org/10.1021/ac061249n

Dentener, F. J., & Crutzen, P. J. (1993). Reaction of N_2O_5 on tropospheric aerosols: Impact on the global distributions of NO_x, O_3, and OH. *Journal of Geophysical Research*, *98*(D4), 7149. https://doi.org/10.1029/92JD02979

Dibb, J. E., Talbot, R. W., & Scheuer, E. M. (2000). Composition and distribution of aerosols over the North Atlantic during the Subsonic Assessment Ozone and Nitrogen Oxide Experiment (SONEX). *Journal of Geophysical Research*, *105*(D3), 3709–3717. https://doi.org/10.1029/1999JD900424

Dibb, J. E., Talbot, R. W., Scheuer, E. M., Blake, D. R., Blake, N. J., Gregory, G. L., et al. (1999). Aerosol chemical composition and distribution during the Pacific Exploratory Mission (PEM) tropics. *Journal of Geophysical Research*, *104*(D5), 5785. https://doi.org/10.1029/1998JD100001

Dillon, M. B., Lamanna, M. S., Schade, G. W., Goldstein, A. H., & Cohen, R. C. (2002). Chemical evolution of the Sacramento urban plume: Transport and oxidation. *Journal of Geophysical Research*, *107*(D5), 4045. https://doi.org/10.1029/2001JD000969

Dubé, W. P., Brown, S. S., Osthoff, H. D., Nunley, M. R., Ciciora, S. J., Paris, M. W., et al. (2006). Aircraft instrument for simultaneous, in situ measurement of NO_3 and N_2O_5 via pulsed cavity ring-down spectroscopy. *Review of Scientific Instruments*, *77*(3), 34,101–34,111. https://doi.org/10.1063/1.2176058

Dunlea, E. J., Decarlo, P. F., Aiken, A. C., Kimmel, J. R., Peltier, R. E., Weber, R. J., et al. (2009). Evolution of Asian aerosols during transpacific transport in INTEX-B. *Atmospheric Chemistry and Physics*, *9*(19), 7257–7287. https://doi.org/10.5194/acp-9-7257-2009

Evans, M. J., & Jacob, D. J. (2005). Impact of new laboratory studies of N_2O_5 hydrolysis on global model budgets of tropospheric nitrogen oxides, ozone, and OH. *Geophysical Research Letters*, *32*, L09813. https://doi.org/10.1029/2005GL022469

Fibiger, D. L., McDuffie, E. E., Dubé, W. P., Aikin, K. C., Lopez-Hilfiker, F. D., Lee, B. H., et al. (2018). Wintertime overnight NO_x removal in a southeastern United States coal-fired power plant plume: A model for understanding winter NO_x processing and its implications. *Journal of Geophysical Research: Atmospheres*, *123*, 1412–1425. https://doi.org/10.1002/2017JD027768

Fisher, J. A., Jacob, D. J., Travis, K. R., Kim, P. S., Marais, E. A., Chan, C., et al. (2016). Organic nitrate chemistry and its implications for nitrogen budgets in an isoprene- and monoterpene-rich atmosphere: Constraints from aircraft (SEAC4RS) and ground-based (SOAS) observations in the southeast US. *Atmospheric Chemistry and Physics*, *16*, 5969–5991. https://doi.org/10.5194/acp-16-5969-2016

Fry, J. L., Draper, D. C., Barsanti, K. C., Smith, J. N., Ortega, J., Winkler, P. M., et al. (2014). Secondary organic aerosol formation and organic nitrate yield from NO_3 oxidation of biogenic hydrocarbons. *Environmental Science and Technology*, *48*(20), 11,944–11,953. https://doi.org/10.1021/es502204x

Fuchs, H., Dubé, W. P., Ciciora, S. J., & Brown, S. S. (2008). Determination of inlet transmission and conversion efficiencies for in situ measurements of the nocturnal nitrogen oxides, NO_3, N_2O_5 and NO_2, via pulsed cavity ring-down spectroscopy. *Analytical Chemistry*, *80*, 6010–6017. https://doi.org/10.1021/ac8007253

Fuchs, H., Dubè, W. P., Lerner, B. M., Wagner, N. L., Williams, E. J., & Brown, S. S. (2009). A sensitive and versatile detector for atmospheric NO_2 and NO_x based on blue diode laser cavity ring-down spectroscopy. *Environmental Science and Technology*, *43*(20), 7831–7836. https://doi.org/10.1021/es902067h

Gerbig, C., Schmitgen, S., Kley, D., Volz-thomas, A., & Dewey, K. (1999). An improved fast-response vacuum- UV resonance fluorescence CO instrument. *Journal of Geophysical Research*, *104*, 1699–1704. https://doi.org/10.1029/1998JD100031

Guo, H., Sullivan, A. P., Campuzano-Jost, P., Schroder, J. C., Lopez-Hilfiker, F. D., Dibb, J. E., et al. (2016). Fine particle pH and the partitioning of nitric acid during winter in the northeastern United States. *Journal of Geophysical Research*, *121*, 10,355–10,376. https://doi.org/10.1002/2016JD025311

Hudman, R. C., Moore, N. E., Mebust, A. K., Martin, R. V., Russell, A. R., Valin, L. C., & Cohen, R. C. (2012). Steps towards a mechanistic model of global soil nitric oxide emissions: Implementation and space based-constraints. *Atmospheric Chemistry and Physics*, *12*(16), 7779–7795. https://doi.org/10.5194/acp-12-7779-2012

Jenkin, M. E., Saunders, S. M., & Pilling, M. J. (1997). The tropospheric degradation of volatile organic compounds: A protocol for mechanism development. *Atmospheric Environment*, *31*(1), 81–104. https://doi.org/10.1016/S1352-2310(96)00105-7

Jenkin, M. E., Saunders, S. M., Wagner, V., & Pilling, M. J. (2003). Protocol for the development of the Master Chemical Mechanism, MCM v3 (Part B): Tropospheric degradation of aromatic volatile organic compounds. *Atmospheric Chemistry and Physics*, *3*, 181–193. https://doi.org/10.5194/acp-3-181-2003

Jenkin, M. E., Young, J. C., & Rickard, A. R. (2015). The MCM v3.3.1 degradation scheme for isoprene. *Atmospheric Chemistry and Physics*, *15*, 11,433–11,459. https://doi.org/10.5194/acp-15-11433-2015

Kercher, J. P., Riedel, T. P., & Thornton, J. A. (2009). Chlorine activation by N_2O_5: Simultaneous, in situ detection of $ClNO_2$ and N_2O_5 by chemical ionization mass spectrometry. *Atmospheric Measurement Techniques*, *2*, 193–204. https://doi.org/10.5194/amt-2-193-2009

Kiendler-Scharr, A., Mensah, A. A., Friese, E., Topping, D., Nemitz, E., & Prevot, A. S. (2016). Ubiquity of organic nitrates from nighttime chemistry in the European submicron aerosol. *Geophysical Research Letters*, *43*, 7735–7744. https://doi.org/10.1002/2016GL069239

LaFranchi, B. W., Wolfe, G. M., Thornton, J. A., Harrold, S. A., Browne, E. C., Min, K. E., et al. (2009). Closing the peroxy acetyl (PA) radical budget: Observations of acyl peroxy nitrates (PAN, PPN, and MPAN) during BEARPEX 2007. *Atmospheric Chemistry and Physics*, *9*(2), 9879–9926. https://doi.org/10.5194/acpd-9-9879-2009

Lee, B. H., Lopez-Hilfiker, F. D., Mohr, C., Kurte, T., Worsnop, D. R., & Thornton, J. A. (2014). An iodide-adduct high-resolution time-of-flight chemical-ionization mass spectrometer: Application to atmospheric inorganic and organic compounds. *Environmental Science and Technology*, *48*, 6309–6317. https://doi.org/10.1021/es500362a

Lee, B. H., Mohr, C., Lopez-Hilfiker, F. D., Lutz, A., Hallquist, M., Lee, L., et al. (2016). Highly functionalized organic nitrates in the southeast United States: Contribution to secondary organic aerosol and reactive nitrogen budgets. *Proceedings of the National Academy of Sciences*, *113*(6), 1516–1521. https://doi.org/10.1073/pnas.1508108113

Lee Ng, N., Brown, S. S., Archibald, A. T., Atlas, E., Cohen, R. C., Crowley, J. N., et al. (2017). Nitrate radicals and biogenic volatile organic compounds: Oxidation, mechanisms, and organic aerosol. *Atmospheric Chemistry and Physics*, *17*(3), 2103–2162. https://doi.org/10.5194/acp-17-2103-2017

Lee, L., Wooldridge, P. J., Gilman, J. B., Warneke, C., De Gouw, J., & Cohen, R. C. (2014). Low temperatures enhance organic nitrate formation: Evidence from observations in the 2012 Uintah Basin Winter Ozone Study. *Atmospheric Chemistry and Physics*, *14*(22), 12,441–12,454. https://doi.org/10.5194/acp-14-12441-2014

Liebmann, J., Karu, E., Sobanski, N., Schuladen, J., Ehn, M., Schallhart, S., et al. (2018). Direct measurement of NO_3 radical reactivity in a boreal forest. *Atmospheric Chemistry and Physics*, *3*, 1–34. https://doi.org/10.5194/acp-2017-975

Liebmann, J. M., Muller, J. B. A., Kubistin, D., Claude, A., Holla, R., Plaß-Dülmer, C., et al. (2018). Direct measurements of NO_3-reactivity in and above the boundary layer of a mountain-top site: Identification of reactive trace gases and comparison with OH-reactivity. *Atmospheric Chemistry and Physics Discussions*, *3*, 1–30. https://doi.org/10.5194/acp-2018-324

Macintyre, H., & Evans, M. (2010). Sensitivity of a global model to the uptake of N_2O_5 by tropospheric aerosol. *Atmospheric Chemistry and Physics*, *10*, 7409–7414. https://doi.org/10.5194/acp-10-7409-2010

Mao, J., Jacob, D. J., Evans, M. J., Olson, J. R., Ren, X., Brune, W. H., et al. (2010). Chemistry of hydrogen oxide radicals (HO_x) in the Arctic troposphere in spring. *Atmospheric Chemistry and Physics*, *10*(13), 5823–5838. https://doi.org/10.5194/acp-10-5823-2010

McDuffie, E. E., Fibiger, D. L., Dubè, W. P., Lopez-Hilfiker, F. D., Lee, B. H., Thornton, J. A., et al. (2018). Heterogeneous N_2O_5 uptake during winter: Aircraft measurements during the 2015 WINTER campaign and critical evaluation of current parameterizations. *Journal of Geophysical Research: Atmospheres*, *123*, 1–28. https://doi.org/10.1002/2018JD028336

Mebust, A. K., & Cohen, R. C. (2014). Space-based observations of fire NO_x emission coefficients: A global biome-scale comparison. *Atmospheric Chemistry and Physics*, *14*(5), 2509–2524. https://doi.org/10.5194/acp-14-2509-2014

Mezuman, K., Bauer, S. E., & Tsigaridis, K. (2016). Evaluating secondary inorganic aerosols in three dimensions. *Atmospheric Chemistry and Physics*, *16*(16), 10,651–10,669. https://doi.org/10.5194/acp-16-10651-2016

Molod, A., Takacs, L., Suarez, M., Bacmeister, J., Song, I. S., & Eichmann, A. (2012). *The GEOS-5 Atmospheric General Circulation Model: Mean climate and development from MERRA to Fortuna*, (Vol. 28). Greenbelt, MD: National Aeronautics and Space Administration, Goddard Space Flight Center.

Neuman, J. A., Parrish, D. D., Trainer, M., Ryerson, T. B., Holloway, J. S., Nowak, J. B., et al. (2006). Reactive nitrogen transport and photochemistry in urban plumes over the North Atlantic Ocean. *Journal of Geophysical Research*, *111*, D23S54. https://doi.org/10.1029/2005JD007010

Nunnermacker, L. J., Kleinman, L. I., Imre, D., Daum, P. H., Lee, Y. N., Lee, J. H., et al. (2000). NO_y lifetimes and O_3 production efficiencies in urban and power plant plumes: Analysis of field data. *Journal of Geophysical Research*, *105*, 9165. https://doi.org/10.1029/1999JD900753

Parrella, J. P., Jacob, D. J., Liang, Q., Zhang, Y., Mickley, L. J., Miller, B., et al. (2012). Tropospheric bromine chemistry: Implications for present and pre-industrial ozone and mercury. *Atmospheric Chemistry and Physics*, *12*(15), 6723–6740. https://doi.org/10.5194/acp-12-6723-2012

Perring, A. E., Pusede, S. E., & Cohen, R. C. (2013). An observational perspective on the atmospheric impacts of alkyl and multifunctional nitrates on ozone and secondary organic aerosol. *Chemical Reviews*, *113*(8), 5848–5870. https://doi.org/10.1021/cr300520x

Ridley, B. A., Walega, J. G., Dye, J. E., & Grahek, F. E. (1994). Distributions of NO, NO_x, NO_y, and O_3 to 12 km altitude during the summer monsoon season over New Mexico. *Journal of Geophysical Research*, *99*(D12), 25,519–25,534. https://doi.org/10.1029/94JD02210

Riedel, T. P., Wagner, N. L., Dubé, W. P., Middlebrook, A. M., Young, C. J., Öztürk, F., et al. (2013). Chlorine activation within urban or power plant plumes: Vertically resolved $ClNO_2$ and Cl_2 measurements from a tall tower in a polluted continental setting. *Journal of Geophysical Research: Atmospheres*, *118*, 8702–8715. https://doi.org/10.1002/jgrd.50637

Rienecker, M., Suarez, M., Todling, R., Bacmeister, J., Takacs, L., Liu, H. C., et al. (2008). The GEOS-5 data assimilation system — Documentation of versions 5.01, 5.1.0, and 5.2.0. NASA Tech. Rep. Ser. Glob. Model. Data Assim., 27, 101.

Rollins, A. W., Browne, E. C., Min, K. E., Pusede, S. E., Wooldridge, P. J., Gentner, D. R., et al. (2012). Evidence for NO_x control over nighttime SOA formation. *Science*, *337*(6099), 1210–1212. https://doi.org/10.1126/science.1221520

Romer, P. S., Duffey, K. C., Wooldridge, P. J., Allen, H. M., Ayres, B. R., Brown, S. S., et al. (2016). The lifetime of nitrogen oxides in an isoprene-dominated forest. *Atmospheric Chemistry and Physics*, *16*(12), 7623–7637. https://doi.org/10.5194/acp-16-7623-2016

Ryerson, T. B., Buhr, M. P., Frost, G. J., Goldan, P. D., Holloway, J. S., Húbler, G., et al. (1998). Emissions lifetimes and ozone formation in power plant plumes. *Journal of Geophysical Research*, *103*(D17), 22,569–22,583. https://doi.org/10.1029/98JD01620

Trainer, M., Angevine, W. M., Brock, C. A., Dissly, R. W., Fehsenfeld, F. C., et al. (2003). Effect of petrochemical industrial emissions of reactive alkenes and NO_x on tropospheric ozone formation in Houston, Texas. *Journal of Geophysical Research*, *108*(D8), 4249. https://doi.org/10.1029/2002JD003070

Saunders, S. M., Jenkin, M. E., Derwent, R. G., & Pilling, M. J. (2003). Protocol for the development of the master chemical mechanism, MCM v3 (Part A): Tropospheric degradation of non-aromatic volatile organic compounds. *Atmospheric Chemistry and Physics*, *3*, 161–180.

Schroder, J. C., Campuzano-Jost, P., Day, D. A., Shah, V., Larson, K., Sommers, J. M., et al. (2018). Sources and secondary production of organic aerosols in the northeastern United States during WINTER. Journal of Geophysical Research: Atmospheres, *123*. https://doi.org/10.1029/2018JD028475

Schumann, U., & Huntrieser, H. (2007). The global lightning-induced nitrogen oxides source. *Atmospheric Chemistry and Physics*, *7*(14), 3823–3907. https://doi.org/10.5194/acp-7-3823-2007

Seidel, D. J., Zhang, Y., Beljaars, A., Golaz, J. C., Jacobson, A. R., & Medeiros, B. (2012). Climatology of the planetary boundary layer over the continental United States and Europe. *Journal of Geophysical Research*, *117*, D17106. https://doi.org/10.1029/2012JD018143

Stone, D., Evans, M. J., Walker, H., Ingham, T., Vaughan, S., Ouyang, B., et al. (2014). Radical chemistry at night: Comparisons between observed and modelled HO_x, NO_3 and N_2O_5 during the RONOCO project. *Atmospheric Chemistry and Physics*, *14*(3), 1299–1321. https://doi.org/10.5194/acp-14-1299-2014

Strapp, J. W., W. R. Leaitch, & P. S. K. Liu (1992). Hydrated and dried aerosol-size-distribution measurements from the Particle Measuring Systems FSSP-300 probe and the deiced PCASP-100X probe. *Journal of Atmospheric Oceanic Technology*, *9*(5), 548–555. https://doi.org/10.1175/1520-0426(1992)009<0548:HADASD>2.0.CO;2

Sutugin, A. G., & Fuchs, N. A. (1970). Formation of condensation aerosols under rapidly changing environmental conditions: Theory and method of calculation. *Aerosol Science*, *1*, 287–293 https://doi.org/10.1016/0021-8502(70)90002-9.

Travis, K. R., Jacob, D. J., Fisher, J. A., Kim, P. S., Marais, E. A., Zhu, L., et al. (2016). Why do models overestimate surface ozone in the Southeast United States? *Atmospheric Chemistry and Physics*, *16*(21), 13,561–13,577. https://doi.org/10.5194/acp-16-13561-2016

Tyndall, G. S., Cox, R. a., Granier, C., Lesclaux, R., Moortgat, G. K., Pilling, M. J., et al. (2001). Atmospheric chemistry of small organic peroxy radicals. *Journal of Geophysical Research*, *106*(D11), 12,157–12,182. https://doi.org/10.1029/2000JD900746

Valin, L. C., Russell, A. R., & Cohen, R. C. (2013). Variations of OH radical in an urban plume inferred from NO_2 column measurements. *Geophysical Research Letters*, *40*, 1856–1860. https://doi.org/10.1002/grl.50267

Wagner, N. L., Dubé, W. P., Washenfelder, R. A., Young, C. J., Pollack, I. B., Ryerson, T. B., & Brown, S. S. (2011). Diode laser-based cavity ring-down instrument for NO_3, N_2O_5, NO, NO_2 and O_3 from aircraft. *Atmospheric Measurement Techniques*, *4*, 1227–1240. https://doi.org/10.5194/amt-4-1227-2011

Wagner, N. L., Riedel, T. P., Roberts, J. M., Thornton, J. A., Angevine, W. M., Williams, E. J., et al. (2012). The sea breeze/land breeze circulation in Los Angeles and its influence on nitryl chloride production in this region. *Journal of Geophysical Research*, *117*, D00V24. https://doi.org/10.1029/2012JD017810

Wagner, N. L., Riedel, T. P., Young, C. J., Bahreini, R., Brock, C. A., Dubé, W. P., et al. (2013). N_2O_5 uptake coefficients and nocturnal NO_2 removal rates determined from ambient wintertime measurements. *Journal of Geophysical Research: Atmospheres*, *118*, 9331–9350. https://doi.org/10.1002/jgrd.50653

Washenfelder, R. A., Wagner, N. L., Dubé, W. P., & Brown, S. S. (2011). Measurement of atmospheric ozone by cavity ring-down spectroscopy. *Environmental Science and Technology*, *45*, 2938–2944. https://doi.org/10.1021/es103340u

Wild, R. J., Edwards, P. M., Bates, T. S., Cohen, R. C., De Gouw, J. A., Dubé, W. P., et al. (2016). Reactive nitrogen partitioning and its relationship to winter ozone events in Utah. *Atmospheric Chemistry and Physics*, *16*(2), 573–583. https://doi.org/10.5194/acp-16-573-2016

Wild, R. J., Edwards, P. M., Dubé, W. P., Baumann, K., Edgerton, E. S., Quinn, P. K., et al. (2014). A measurement of total reactive nitrogen, NO_y, together with NO_2, NO, and O_3 via cavity ring-down spectroscopy. *Environmental Science and Technology*, *48*(16), 9609–9615. https://doi.org/10.1021/es501896w

Wilson, E. W., Hamilton, W. A., Kennington, H. R., Evans, B., Scott, N. W., & Demore, W. B. (2006). Measurement and estimation of rate constants for the reactions of hydroxyl radical with several alkanes and cycloalkanes. *Journal of Physical Chemistry A*, *110*, 3593–3604. https://doi.org/10.1021/jp055841c

Yamartino, R. J. (1984). A comparison of several "single-pass" estimators of the standard deviation of wind direction. *Journal of Applied Meteorology and Climatology*, *23*(9), 1362–1366. https://doi.org/10.1175/1520-0450(1984)023<1362:ACOSPE>2.0.CO;2

York, D., Evensen, N. M., Martínez, M. L., & De Basabe Delgado, J. (2004). Unified equations for the slope, intercept, and standard errors of the best straight line. *American Journal of Physics*, *72*(3), 367–375. https://doi.org/10.1119/1.1632486